We are IntechOpen, the world's leading publisher of Open Access books Built by scientists, for scientists

4,800
Open access books available

122,000
International authors and editors

135M
Downloads

Our authors are among the

154
Countries delivered to

TOP 1%
most cited scientists

12.2%
Contributors from top 500 universities

CLARIVATE ANALYTICS BOOK CITATION INDEX INDEXED

WEB OF SCIENCE™

Selection of our books indexed in the Book Citation Index in Web of Science™ Core Collection (BKCI)

Interested in publishing with us?
Contact book.department@intechopen.com

Numbers displayed above are based on latest data collected.
For more information visit www.intechopen.com

Chapter

Nanoplasmonic Arrays with High Spatial Resolutions, Quality, and Throughput for Quantitative Detection of Molecular Analytes

Rishabh Rastogi, Matteo Beggiato, Pierre Michel Adam, Saulius Juodkazis and Sivashankar Krishnamoorthy

Abstract

Recent developments in nanoplasmonic sensors promise highly sensitive detection of chemical and biomolecular analytes with quick response times, affordable costs, and miniaturized device footprints. These include plasmonic sensors that transduce analyte-dependent changes to localized refractive index, vibrational Raman signatures, or fluorescence intensities at the sensor interface. One of the key challenges, however, remains in producing such sensors reliably, at low cost, using manufacturing compatible techniques. In this chapter, we demonstrate an approach based on molecular self-assembly to deliver wafer-level fabrication of nanoplasmonic interfaces, with spatial resolutions down to a few nanometers, assuring high quality and low costs. The approach permits systematic variation to different geometric variables independent of each other, allowing the significant opportunity for the rational design of nanoplasmonic sensors. The ability to detect small molecules by SERS-based plasmonic sensing is compared across different types of metal nanostructures including arrays of nanoparticle clusters, nanopillars, and nanorod and nanodiscs of gold.

Keywords: nanofabrication, self-assembly, nanoplasmonic sensor, nanoarray, nanoclusters, nanopillar, nanoparticle, hot spots

1. Introduction

The optical properties of metal nanostructures and nanoarrays have been widely investigated in the context of exploiting particle plasmons to derive high performance within chemical and biosensing devices. These include sensing of range of analytes to diagnose the medical status of an individual [1]; detect the presence of chemical or biowarfare agents [2, 3], toxins, or adulterants in food [4]; or assess/monitor air, water, and soil quality in the environment [2, 5]. Plasmonic sensors offer a range of advantages over other analytical tools including high analytical and calibration sensitivity, quick response times, label-free detection opportunities, ease of integration within different sensor form factors, and the need for simple and portable instrumentation. Plasmonic sensors rely on

metal nanostructures that act as nanoantennae to concentrate and enhance the electromagnetic field close to surface [6]. The enhanced EM field can be leveraged within different configurations, namely, localized surface plasmon resonance sensors (LSPR) that follow analyte-induced changes to local refractive index or report vibrational Raman or fluorescence intensities with high signal-to-noise ratios using surface-enhanced Raman spectroscopy (SERS) and metal-enhanced fluorescence (MEF), respectively. In all these cases, the performance of the sensor is critically linked to the optical properties of the plasmonic structures, which in turn correlates with their geometric attributes, namely, size, shape, aspect ratios, separation, distribution, and roughness. Control over geometries is the key to engineering profiles and intensities of the electromagnetic field around plasmonic nanostructures, which in turn determines the performance of the plasmonic transducer. The typical length scales for characteristic dimensions of plasmonic nanostructures correspond to spatial resolutions of few nanometers to few tens of nanometers. Geometric features such as pointed structures or nanoscale gaps have shown to concentrate and enhance EM field, thus acting as EM hot spots, as a function of decreasing radius of curvature or gap distances, with length scales down to sub-10 nm regime [7]. Enhanced EM fields at gap hot spots have shown to result in enhancement factors of the order of a million- to billion-fold in practice. A sizeable contribution to observe SERS signals (24% of the overall intensity) was observed to be rising out of <100 molecules per million when these molecules are positioned in EM hot spots with EM enhancement factors of the order of 10^9–10^{10} [8]. The EM hot spots help enhance the sensitivity of different plasmonic sensors, and especially those based on enhanced spectroscopies, namely, SERS and MEF. Gaining high sensitivity would thus be largely determined by the quality and number of EM hot spots [9]. However, addressing the production of EM hot spots with length scales of the order of only a few nanometers pose a profound and non-trivial challenge for nanofabrication. Traditionally, such hot spots have been attained as a natural consequence of stochastic growth or deposition processes [10, 11], including electrochemical growth or roughening, de-wetting of nanoparticles or salts from solution phase [12–14], and de-wetting of thin films on the surface. The stochastic processes, by nature, result in a broad standard deviation in geometries, which reduces the number of most efficient hot spots and also leads to greater spot-to-spot variability in signal intensities [15, 16]. The randomness in geometry makes it particularly hard to predict response, to identify the source of issues, and to adopt a rational approach to optimize performance. Geometries with improved definition have remained forte of top-down lithography tools, for example, E-beam lithography, focused ion-beam milling, and X-ray interference lithography, which are all very time-consuming and also quite expensive [17–19]. The throughput and cost of fabrication is not only an issue for manufacturing but also reduces the efficacy of research due to the limitation in the number of samples available for investigations [20] (**Figure 1**). From the manufacturing perspective, the throughput of the process would be a key determinant of the cost, which is driven to <$5 per sensor chip for point-of-care applications [28].

Techniques such as nanoimprint lithography and polymeric or colloidal self-assembly techniques allow enhancing throughput, albeit, at the cost of defects. The ability of self-assembly techniques in catering to the parallel fabrication of nanopatterns across arbitrarily large areas at low cost, as well as the several handles it offers toward tunability of structure dimensions down to molecular level, is unmatched by conventional lithography tools. However, self-assembly-based approaches carry limitations that demand careful attention to ensure their

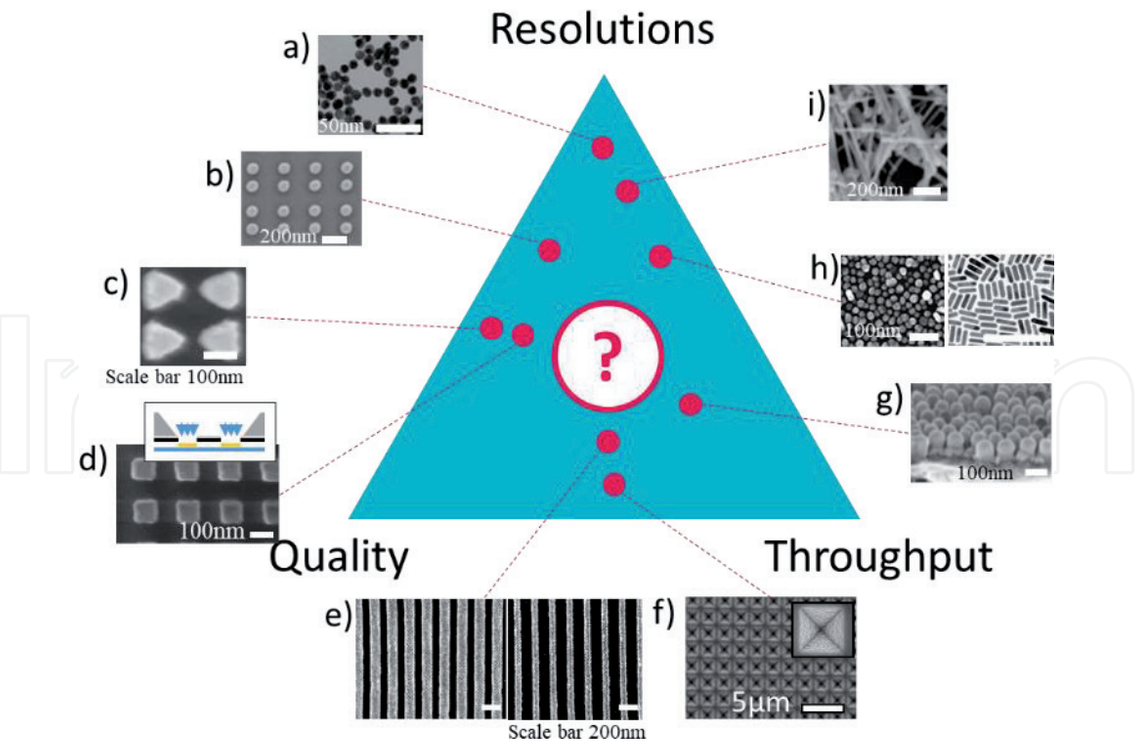

Figure 1.
Schematic representation of the trade-off between resolution, quality, and throughput in fabricating plasmonic nanoarrays with high spatial resolutions, showing the comparative advantages and limits of (a) nanoparticle assemblies [21] (b) top-down-bottom-up control over nanoparticle assemblies [19], (c) direct-write techniques [22], (d) nanostencil lithography [23], (e) nanoimprint lithography [24], (f) photolithography [25], (g) porous anodized alumina templates [10], and (h) stochastic, random structures, including island films [11, 26], and (i) stochastic chemical growth processes [27].

usefulness: (a) Poor uniformity, which is often a result of poor process optimization and in some cases due to the susceptibility of process parameters to environmental variables. This can be addressed by mapping the impact of environmental variables and factoring them within the process optimization. (b) Large standard deviations, either inherent to the primary templates produced by the technique or those that may creep in during different stages of processing. (c) Feature shape: Typically, self-assembled template patterns have a circular feature cross section. Rectangular, triangular, or other feature shapes with lower symmetry are uncommon. (d) In the absence of any external guidance, self-assembly techniques typically lead to a polycrystalline 2D hexagonal order. Long-range ordering, square, or other lattice types besides hexagonal symmetry remain uncommon and can be attained through guidance from a top-down lithographic tool [29–34]. The lack of long-range order and presence of point or line defects are better tolerated by plasmonic sensing applications, so long as the averaged properties are consistent and reproducible with low standard deviations. The chapter will present our approach to plasmonic nanoarrays with high spatial resolutions relying on hierarchical self-assembly of amphiphilic di-block copolymers into soft colloids and their subsequent quasiperiodic organization when deposited on a planar surface [35]. The approach results in well-defined organic templates on the surface with nanometric control over the width, topography, and pitch, realized by control over parameters of molecular self-assembly. By understanding the impact of the different process parameters on the resulting geometric outcome, it is possible to deliver templates with high reproducibility and uniformity on full wafers, with a yield >90% [36]. These templates are translated into highly sensitive SERS-based plasmonic sensors, with control over metal nanogaps down to sub-10 nm regime.

2. Spatially controlled fabrication of nanoscale templates

2.1 Fabrication of self-assembled templates

Amphiphilic di-block copolymers can self-assemble into reverse micelles when dissolved in a solvent that selectively dissolves only the apolar block of the copolymer. These reverse micelles can be obtained or be induced into attaining a spherical morphology, with a feature size determined by their aggregation number. The micelle aggregation number is not only a function of the molecular weight and composition of the copolymer but also the quality of the solvent used and the presence of additives. As a consequence, the size can be varied independent of the molecular weight, using solvent quality and concentration of additives as useful handles to fine-tune template geometries and eventually those of resulting plasmonic arrays. The spherical micelles are solvent-laden colloidal structures which can be readily organized on a variety of surfaces to yield a 2D hexagonally ordered dot-array templates. These templates are subjected to physical or chemical means of pattern transfer to produce nanopatterns of desired materials. Pattern formation on surfaces using copolymer reverse micelle approach is fundamentally different from that of microphase separation in block copolymer thin films [37–39]. The size of reverse micelles in solution, which eventually determines the feature sizes on the surface, is independently variable by engineering the solvent quality or the use of additives. The standard deviation of the templates on the surface is determined by that of the micelles in solution phase before deposition, which in turn is governed by the intermicellar exchange process. The exchange process is slow due to the slower diffusion for larger molecular weight polymers or when solvent with high selectivity to the corona-forming blocks is employed [40]. During the spin-coating process, the solvent-laden micelles in solution deform on the surface to assume an ellipsoidal shape, with partial fusion of corona from adjacent reverse micelles resulting in the globally continuous organic film presenting periodic contrast in topography with an ultrathin film (<5 nm) in the background. The pitch of the ensuing pattern on the surface can be varied in steps <5% of its mean value, through control over evaporation rate or the concentration of the micelles in solution. The evaporation rate can be controlled using spin or dip coating speeds. The ability to vary the lattice periodicity within a certain window is attributed to a range of distances for which the PS blocks from the corona of adjacent micelles can still meet upon deformation and film formation. When this condition is not met, namely, at low solution concentrations or high spin speeds, the reverse micelles are spaced too far apart, resulting in patchy coverage. On the other hand, at high solution concentrations or at low spin speeds, the excess concentration beyond what is necessary toward a monolayer appears as multilayers [36]. The topography of the reverse micelle film is a variable that can be determined by the relative humidity in the ambient environment during the coating process. This is attributed to the change in moisture that is likely to concentrate at the polar core-forming PVP and consequently increasing the interfacial tension resulting in resistance to collapse and as a result a higher topography. Under optimal conditions of coating, micelle arrays can be produced with a standard deviation of <10% in geometric attributes across a complete wafer.

In a specific example shown in **Figure 2**, reverse micelles of polystyrene-block-poly (2-vinylpyridine) (PS-b-P2VP) are obtained from dilute solutions of m-xylene. Here, a copolymer with a molecular weight of 81.5 kDa and a PDI of 1.10, at a concentration of 0.5% w/w in m-xylene, is spin-coated on a clean silicon surface at 5500 rpm resulting in a hexagonally ordered array with feature heights of 20 nm and pitch of 66 nm with typical standard deviations <15% in all geometric

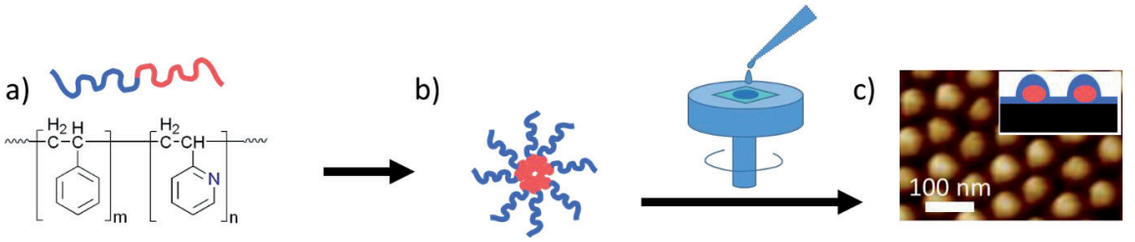

Figure 2.
Schematic representation of the self-assembly of amphiphilic di-block copolymer into reverse micelles and their subsequent assembly to form two-dimensional arrays on the surface.

variables. During the spin-coating process, the solvent-laden micelles in solution deform on the surface to assume an ellipsoidal shape, with the corona from adjacent reverse micelles coming together resulting in the globally continuous thin film presenting periodic topography and ultrathin film (<5 nm) in the background. The center-to-center distance or the pitch of the template arrays could be systematically decreased in steps of <5 nm between 45 and 60 nm by increasing the solution concentrations from 0.6 to 1% at a fixed spin-speed of 5000 rpm or decreasing spin-speeds from 9000 to 2000 rpm at a fixed concentration of 0.7%. The ranges were found to constitute an optimal window of conditions where a continuous uniform film was obtained.

2.2 Reproducibility and scalability

Among key limitations encountered by self-assembly-based approaches, in general, is the scaling up to practically large areas while ensuring high consistency and reproducibility. The issues of reproducibility arise mainly due to the sensitivity of the process outcome to environmental parameters. Such sensitivity also limits process scalability, due to inconsistencies encountered when coating large areas like full wafers and to limited batch-to-batch reproducibility. These issues are true also for the case of self-assembly of amphiphilic copolymers, and this can be addressed only by adequate investigations directed at mapping the impact of different environmental variables on the process outcomes. Several sources of variability were identified and addressed for the self-assembly of amphiphilic copolymers, including the presence of moisture and contaminants in solution; history of preparation (agitation and incubation), temperature, and humidity; differences in surface roughness or surface energy (e.g., due to organic or particulate contaminants on the surface); changes to solution concentrations due to solvent evaporation during use; and inadequate mixing of polymer. Under optimal conditions, the assemblies of reverse micelle feature exhibit standard deviations lower than 15% across full wafers.

A specific outcome of optimization of the templates represented in **Figure 2c** on a 100 mm silicon wafer can be seen in **Figure 3**, which shows the distribution for height, diameter, pitch, and nearest neighbors, at different regions of the wafer. Typical characterization involves AFM topography for heights and diameters (within errors of AFM tip-convolution) and SEM top view and image analysis using ImageJ or MATLAB. A representative AFM image recorded in the tapping mode is shown in **Figure 3b**. The characterization is critical for each batch of samples, and it is possible to scale the process to several batches of wafers [41]. Points A, B, C, and D correspond to four positions representing systematically increasing radial distances from the center to the edge of the wafer. AFM measurements at these points show standard deviation <15% for geometric variables and <10% variation of their mean values across the full wafer. Voronoi analysis of the AFM images shows a predominance of

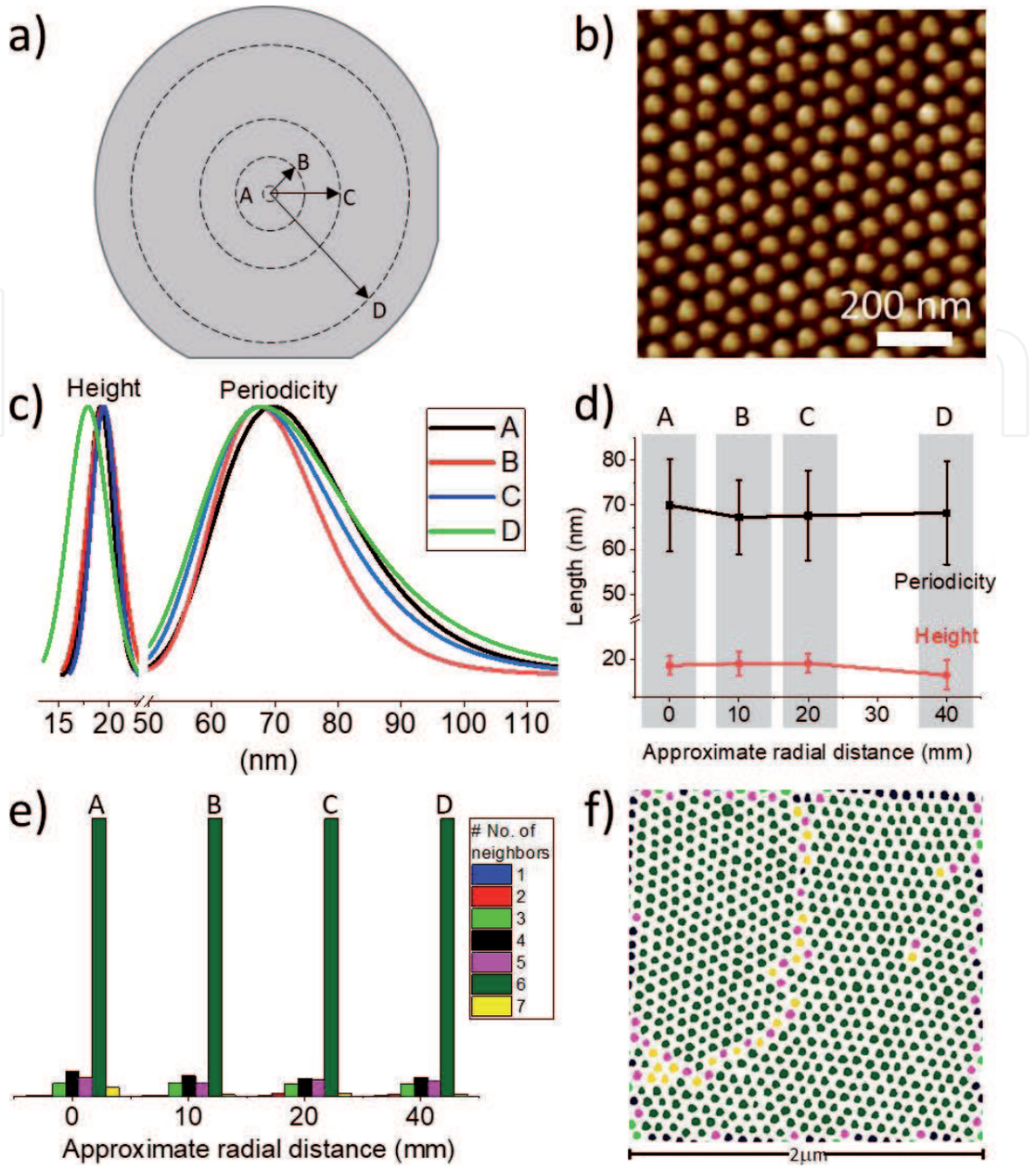

Figure 3.
Demonstration of scalability combined with uniformity on full wafers of optimized coatings: (a) Schematic of radially separated points from center to edge of 100 mm wafer, (b) where tapping mode AFM measurements are performed (image indicated for point a), (c) the distribution of height and pitch across full wafer, (d) with mean values plotted as function of radial distance from center, and error bars showing standard deviation in corresponding feature dimensions at a single point, (e) histogram of nearest neighbors showing predominantly six nearest neighbors as expected for hexagonal assembly, maintained across the wafer, and (f) representation of nearest neighbors using Voronoi analysis, with the features colored corresponding to the number of nearest neighbors as indicated in (e).

six nearest neighbors as expected for hexagonal packing, which is uniformly maintained across the wafer (**Figure 3e, f**). The outcome clearly demonstrates the feasibility for reliable scaling up of the technique to cater to nanostructures over large areas.

3. Nanoplasmonic arrays by pattern transfer

Fabrication of plasmonic nanoarrays starting from organic templates relies on pattern transfer approaches, for example, template-guided growth, deposition, or etching, to define noble metal nanoarrays with the conservation of pitch from

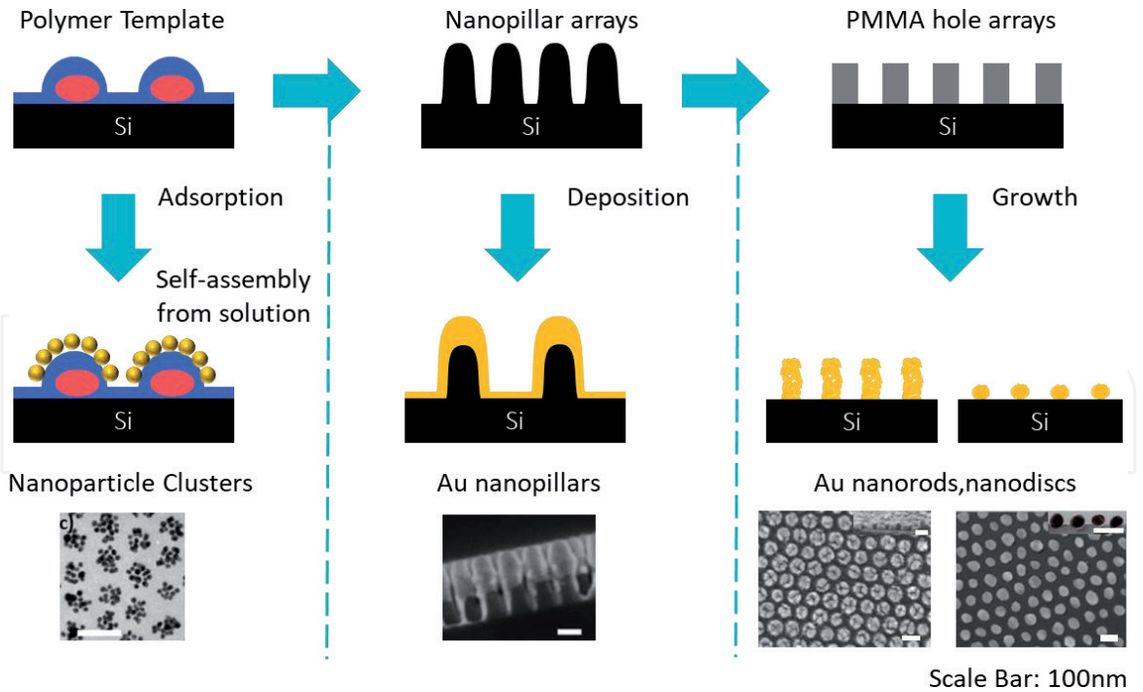

Figure 4.
Fabrication of plasmonic nanoarrays with different profiles, size, and distributions of metal nanostructures can be attained by control over pattern transfer processes. In all cases, the advantages of the original templates including the uniformity and scalability are preserved [42–44].

the original template. The pattern transfer approaches offer large flexibility in the geometry of the individual features, thus making it possible to fabricate plasmonic nanoarrays of different types, for example, nanoparticle cluster arrays, nanopillars arrays, nanorods, or nanodiscs. The pattern transfer parameters provide independent control over the size, shape, and aspect ratio of the features and should be optimized to ensure that they do not affect the spatial arrangement, uniformity, and reproducibility from the original template. Although the pattern transfer approaches are common in semiconductor fabrication, extending them to work at the scale of few nanometers requires rigorous optimization and quality assurance to ensure low standard deviations and reproducibility in geometries. Further in this section different pattern transfer methods to reach such three different plasmonic nanoarrays have been discussed in detail (**Figure 4**).

3.1 Nanoparticle cluster arrays

Clusters (used interchangeably with "aggregates" in this report) of metal nanoparticles behave differently from their isolated counterparts due to the collective optical behavior arising out of plasmonic coupling between the constituent nanoparticles [45–50]. Clusters of nanoparticles are known to behave as hot particles, with significantly enhanced electromagnetic fields at the inter-particle junctions [51–54]. Consequently, clusters exhibit higher extinction cross sections, with hot spots that can be excited at lower energies than the isolated particles. The aggregation-induced color change of gold nanoparticle suspensions caused by the analyte of interest has been the basis of several biological assays [55]. Such random aggregation typically results in a large distribution in the number of particles per cluster, with a distinct lack of control over those numbers. To achieve clusters with desired optical properties, it is essential to be able to produce them with a narrow distribution in the size, shape, and spatial arrangement between nanoparticles within the cluster and between clusters in an array. Such clusters were demonstrated using templates

fabricated by electron- beam lithography (EBL) [45–47, 53, 56–58] and controlling the size of the template to obtain dimers, trimers, quadrumers, and multimers. Since EBL is time-consuming and expensive to achieve high-resolution patterns spanning large areas, other low-cost means to achieve controlled nanoparticle aggregates using template-assisted means have been reported in the literature. These include the use of DNA, [59] surfactants, [60] block copolymers [60–62], carbon nanotubes [61], cylindrical micelles [62], or microorganisms like bacteria or viruses [63] as templates to attach nanoparticles. While the template-assisted cluster formation allows creating clusters with desired size (or a number of particles per cluster) and shape, they often fall short of abilities to control inter-cluster arrangement within an array. Such an arrangement is important to ensure reproducible inter-cluster plasmonic interactions as well as an ability to engineer them to achieve desired optical properties. In this direction, block copolymers are an excellent solution, as they allow effective control over the spatial arrangement of eventual clusters. Microphase separation of block copolymers (BCP) in thin films, as well as BCP reverse micelles, has been utilized as templates to attain clusters of metal nanoparticles on surfaces. These techniques have exploited the BCP templates either to organize one or more particles from solution phase [64–66] or to drive selective complexation of metal ions and in situ reduction to form clusters [67]. However, these fall short of opportunities for the rational design of the cluster properties. The approach based on copolymer reverse micelle template allows preparing clusters based on electrostatic self-assembly of preformed gold nanoparticles from the solution phase on to the features on the surface. The cluster dimensions (the number of nanoparticles per cluster) and the inter-cluster separation were controlled by control over the template size and their separation. The low standard deviation of the template enables low standard deviation in the geometric attributes of the clusters as well (**Figure 5**).

In a typical experiment, the reverse micelle arrays prepared from PS-b-PVP with a molecular weight of 114 kDa and PDI of 1.1 were spin coated from m-xylene solutions and subsequently exposed to an aqueous suspension of gold nanoparticles. Due to the presence of the pyridyl groups of PVP in the core of the features, the reverse micelle features are positively charged and attract negatively charged citrate-stabilized gold nanoparticles from the suspension. The electrostatic attraction between the nanoparticles occurs locally on the features and not in between them, therefore resulting in a patterned array of nanoparticle clusters. The number of nanoparticles in each feature is a function of its size. The inter-cluster separations are controlled by the control over the pitch of the template. Extinction spectra of the nanoparticle clusters showed a peak at 620 nm, which was over 100 nm red-shifted from the plasmon resonance band of isolated Au nanoparticles. This is attributed to the strong plasmonic coupling between the nanoparticles within the cluster. Further, the absence of a strong contribution at 520 nm would confirm the geometric observation of the absence of isolated nanoparticles (**Figure 6**). Finite-difference time-domain (FDTD) simulations show inter-particle as well as inter-cluster hot spots. The 3D shape of the clusters was found to be necessary for the inter-cluster plasmonic coupling, and an increase in EM field at inter-particle and inter-cluster hot spots was found to correlate with decreasing inter-cluster separations. The expectations from the geometry and optical properties of the nanoparticle cluster arrays were validated by SERS measurements of a probe molecule. Three different probe molecules were tested, namely, crystal violet, naphthalene thiol, and 2, 2′-bipyridine. In all three cases, the SERS intensities were found to be highest for the largest clusters with the smallest separations. The SERS intensities were higher for crystal violet than for smaller molecules due to resonance Raman effects, enabling SERS enhancement factors over 10^8. SERS quantitative assays showed the

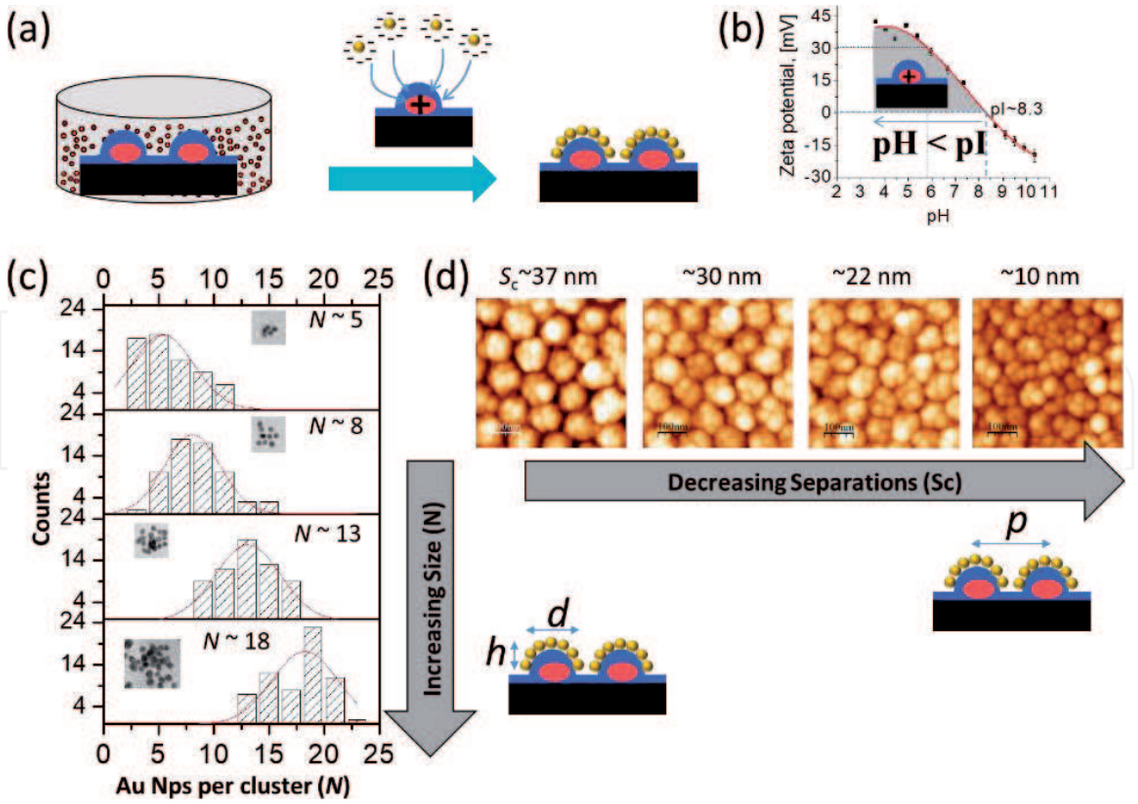

Figure 5.
(a) Schematic of the fabrication of gold nanoparticle cluster arrays by electrostatic attraction of negatively charged Au nanoparticles to positively charged templates on surface, (b) zeta potential titration showing the template acquiring positive potential for pH below 8.3, (c) systematic control over the size (pitch kept a constant), and (d) separation (S_c) between the nanoparticle clusters (size kept a constant at N~18) which is shown by the histograms and AFM measurements, respectively [42].

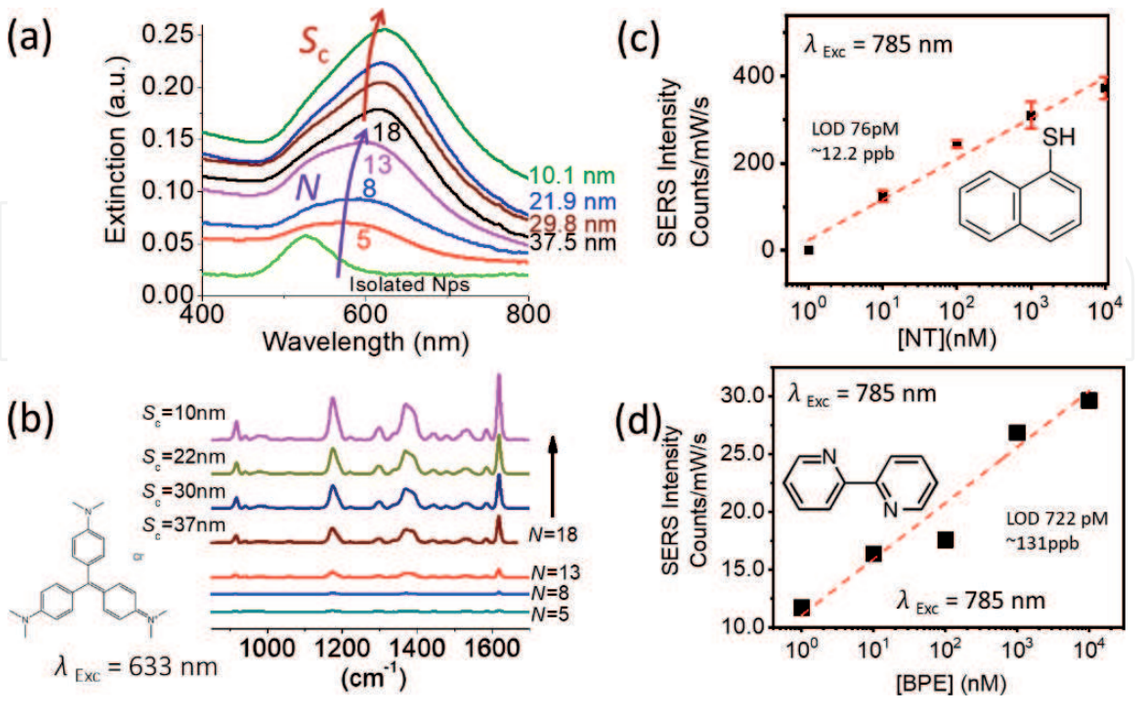

Figure 6.
(a) Graph shows the shift in the extinction peak of the nanoparticle clusters with change in separation, Sc, and change in no. of nanoparticles/cluster, N. (b) SERS spectra of CV shows the increase in the peak intensity at 1625 cm^{-1} with change in the separations, Sc, and no. of nanoparticles/cluster, N. (c) and (d) SERS intensity vs. concentration showing linear relationship for 1-NT and BPE, respectively [42].

lowest detection limits for naphthalene thiol to be an order of magnitude lower than 2,2′- bipyridine. This is attributed to the higher density of molecules for naphthalene thiol on the surface due to the covalent bonding of the thiols to the gold surface at a given concentration. The low standard deviations of the cluster arrays enabled signal intensity variations below 10% on several square millimeters on the surface.

3.2 Metal nanopillars arrays

Nanopillar shapes offer a unique opportunity to control and enhance EM field profiles and enhancements [68]. Nanopillar arrays for plasmonic sensing have been reported previously in the literature, for detection of disease markers and identification of bacteria as well as environmental pollutants [43, 69–71]. Such configurations can be obtained by metal deposition of optimal thickness on top of high aspect ratio dielectric pillars that can be produced by different approaches, namely, VLS growth [72], pulsed laser deposition [73], black Si production by RIE with gas plasmas [74], and patterned wet or dry etching with templates produced by other means, for example, photolithography, soft-lithography, EBL, NIL, NSL, and molecular self-assembly [75–80]. Nanopattern of pillars offers an advantage over stochastically arranged counterparts due to a better definition of the spatial relationship between the pillars that help rational enhancement to sensing performance. The stochastic arrangements, despite promising results, rely largely on empirical optimization and suffer from difficulty in identifying issues when they arise. Another aspect to consider is the stability of the pillar arrays, which is especially a concern for high aspect ratio structures [81–84]. High aspect ratio pillars can capture analyte between the pillars when they collapse by drying that may offer interesting means to trap analyte potentially at EM hot spots [85, 86]; the approach, however, gives less control over the collapse nor the concentration of analyte that is trapped, thus offering limited opportunity for rational design. The irreversible nature of such collapse would make it difficult to subject the pillars to solvent-based washing and drying steps, limiting them to a single time or single-step usage. Pillars of smaller aspect ratios would solve many of these issues,; however, it will need to be produced with high spatial resolutions to ensure a large number of EM hot spots and preferably with good geometric definition allowing rational optimization toward both enhancing EM hot spots and analyte capture on the surface. An approach based on colloids of amphiphilic copolymers allows the possibility to generate nanopillars that are stable and reusable while allowing significant opportunities to rationally engineer the optical properties toward high plasmonic sensing performance.

Organic reverse micelle templates can be transferred into the underlying Si by adopting nanolithography processes based on reactive ion etching with halogen gas plasmas. Given the low template thickness (typically less than 30 nm) and small widths (sub-100 nm), nanolithography using these templates requires significant process optimization to ensure high selectivity to the underlying substrate, minimum undercut, and high anisotropy. It is possible to substitute the organic templates with a harder inorganic template to improve the selectivity and durability. This is achieved by transferring the organic template pattern into a thin dielectric film to generate harder dielectric masks for the next step of pattern transfer into Si. We had earlier shown a high degree of control over the incorporation of the organometallic precursor by using atomic layer deposition, with the resulting oxide nanostructures enabling nanolithography down to sub-10 nm regime [35]. This was followed by several other investigations in literature focusing on vapor phase incorporation of metal-organic precursors within different block copolymer

domains using ALD processes [87–91]. It is important that the nanolithography process is optimized to not widen standard deviations between the features or across the wafer. The optimization processes across the full wafer level should take into account the "loading effects," which impacts the outcome of the reactive ion etching process depending on the proportion of exposed surface area available for etching.

Nanopillar arrays that are shorter and closer allows all advantages of the other reported approaches, while in addition also conserving the metal to be deposited. Nanopillar arrays of silicon obtained by molecular self-assembly approach (**Figure 8**) can subsequently be coated with gold or silver to prepare plasmonic nanopillar arrays. The conditions of the coating, including the choice of evaporation versus sputtering, the respective deposition parameters are critical to the structure and property of the resulting plasmonic arrays. The thickness of the films deposited in relation to the geometry of the underlying silicon pillars would be a key process parameter that determines the aspect ratio and the separation between the metal pillars. Both aspect ratio and the feature diameters increase, while the feature separations decrease systematically as a function of the thickness of metal deposited. The observed film growth is strongly anisotropic with slow growth laterally as compared with vertically. The growth on top of the silicon pillars correlates well with the thickness of the metal deposited, while the increase in diameter occurs much slower. The challenge in the processing includes the conformal deposition of metal, with good step edge coverage, especially when the deposition is made on top of closely separated high aspect ratio nanopillars.

In a specific example, organic templates prepared using PS-b-PVP with a molecular weight of 80.5 kDa was spin-coated on a 100mm Si wafer consisting of a 25 nm film of thermally grown SiO_2 layer (**Figure 7a**). The coating is exposed to brief O_2 plasma to remove the thin residual layer between the template features and expose the substrate beneath. The resulting organic template is then transferred into an underlying SiO_2 thin film using C_4F_8/CH_4 gas plasma. The resulting SiO_2 islands provide high selectivity in etching underlying Si using SF_6/C_4F_8 plasma to yield Si nanopillars. The RIE conditions employed resulted in silicon pillars with a positively tapered profile with a feature size of 40 nm (at half-width) and pitch of 78 nm and height of 120 nm, as measured by SEM (**Figure 7b**). The RIE process conditions can be varied to obtain pillars with other shapes as well (**Figure 7c**). The pillar arrays were found to be uniform throughout the wafer, as qualified by uniform color, with a variation of <10% as measured by reflectance spectroscopy [35]. **Figure 8** shows another case of similarly obtained nanopillars arrays prepared using

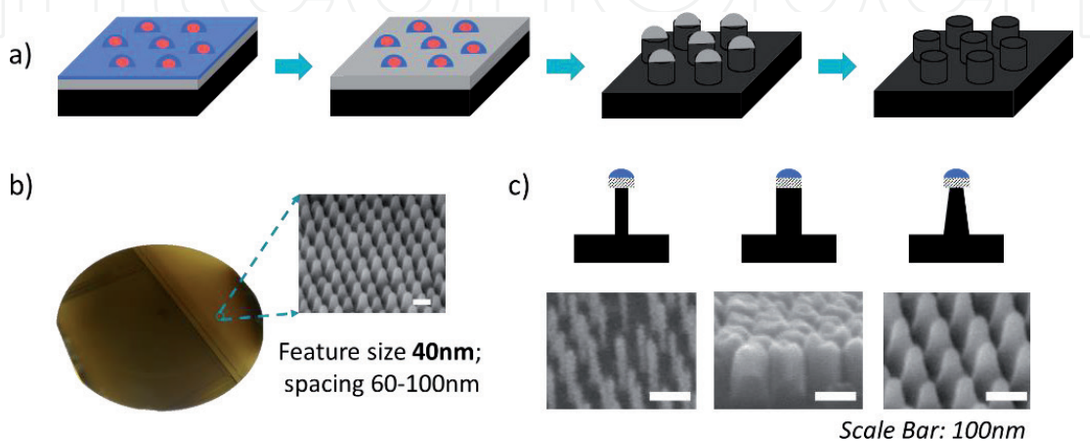

Figure 7.
(a) Fabrication process involved in pattern transfer from polymer template to fabricate silicon nanopillar arrays. (b) SEM image taken from a random position on the wafer with nanopillar arrays. (c) SEM images of different shapes of nanopillars obtained by varying etching conditions [35].

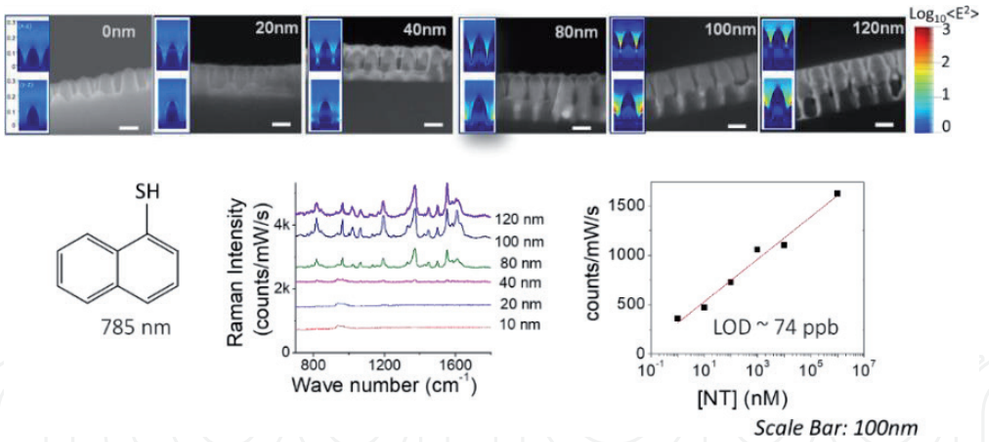

Figure 8.
(Top) Silicon nanopillar arrays with increasing thickness of gold (top, insets) show evolution in electromagnetic field profiles (bottom, left) and SERS spectra of 1-naphthalene thiol as function of metal pillar geometry (bottom, right) concentration dependence of intensity of the peak at 1371 cm^{-1} showing quantitative detection with low detection limits [43].

a different PS-b-P2VP (114 kDa, PDI - 1.1, fPS ~0.5) system. The Si pillar arrays are converted to plasmonic nanoarrays bycoating with thin layer of Cr, followed by systematically increasing thicknesses of gold by electron beam evaporation. The nanopillars coated with 5 nm Cr/120 nm of Au were found to result in gold pillars with separations below 10 nm. The optical modeling of the nanopillars proved EM hot spots with increasing intensity and with increasing metal thickness, as expected. This was correlated well with SERS experiments of 1-naphthalene thiol, where the evolution in SERS intensity was found to saturate at 100 nm. SERS-based plasmonic assays of naphthalene thiol show analytical sensitivity down to 74 ppb, low standard deviations in SERS intensities for different concentrations, and feasibility for quantification with large dynamic range. The approach established clear control over structure, property, and function to optimize the final performance of the plasmonic sensor.

3.3 Nanorods and nanodisc arrays from nanoimprint lithography from self-assembly derived high-resolution masters

The uniform templates obtained using reverse micelle approach is well-suited as masks for nanolithography to produce Si nanopillar arrays. These nanopillar arrays are highly interesting for exploitation as high-resolution molds for nanoimprint lithography (NIL) [44]. NIL is a convenient top-down patterning tool that allows replication of surface relief structures down to sub-10 nm feature sizes present in a mold into the polymer substrate [24, 92]. Replication using the NIL process is achieved by pressing the mold against a molten polymer film, followed by solidifying the polymer either by cooling below its Tg or by cross-linking, before removing the mold. Among the several top-down techniques known, NIL has particularly recognized as manufacturing compatible, scalable and low-cost solution for fabricating nanoscale templates of high resolution. The use of the silicon nanopillar arrays as NIL molds offers a distinct advantage of producing multiple copies of templates with identical pitch and width as the original pillars. Since these templates are used to produce metal arrays in the next step, it is possible to attain asymmetric metal features, with reproducibility in optical properties within and between samples. In a specific example, full wafers consisting of Si nanopillar arrays with a height of 120nm were fabricated as described in Section 3.1. They were subsequently diced into smaller pieces and used as NIL molds to replicate the pillar arrays into a thin

film of PMMA (100 nm thick) coated on Si substrate. Prior to imprinting, the pillar arrays are functionalized with a perfluorosilane layer to enable anti-stiction property. The NIL process results in a nanoporous PMMA film with geometric characteristics that match with the Si pillar array mold (**Figure 9**). The pores were found to be ~120 nm deep, with a residual layer of ~10 nm thickness present beneath the pores. The residual layer was removed using a controlled O_2 plasma exposure and treated with HF in order to expose the bare Si substrate beneath. The porous template with through-holes was subsequently employed to guide the growth of metal to achieve gold nanorods from the surface through an electroless deposition process. The electroless deposition of gold was performed by galvanic displacement reaction where the oxidation of silicon substrate by HF provides electrons to reduce the Au(III) ions to Au(0), in a process earlier shown by Aizawa et al. [93, 94]. Exposure of the nanoporous template to an electroless plating bath consisting of 0.9% HF and 2.3 mM of $HAuCl_4$ for a duration of 1 min was sufficient to grow the nanorods within the pores. The selectivity of the process to the Si substrate ensured the absence of any non-specific metal deposition in unintended areas. The nanoporous PMMA template was then removed using an O_2 plasma exposure. The Au nanorod arrays were found to be 80 nm in height with a pitch identical with that of the NIL mold used. Upon annealing the nanorod array at 200°C for 2 h, a transformation in morphology into nanodiscs was observed. Such transformation that was observed to occur significantly below the melting point of bulk gold metal is likely due to compacting of nanoparticulate and porous gold features obtained upon electroless deposition. The nanoparticulate nature of nanorods is evident from the SEM measurements. The nanodiscs exhibit an ellipsoidal shape, with a diameter of 55.2 (± 4) nm and height of 35.3(± 5.4) nm, as measured using SEM and AFM. TEM cross section of the nanodisc arrays shows that the discs were present within depressions on the surface with a depth of ~5 nm. The depression below the nanodisc is presumably formed by substrate etching, due to the presence of HF in the electroless chemical bath. The transformation of the rod to disc morphology was found necessary in order to ensure mechanical stability of the metal arrays when exposed to solvents. It was found that the nanorod arrays disintegrated when dipped in aqueous solutions,

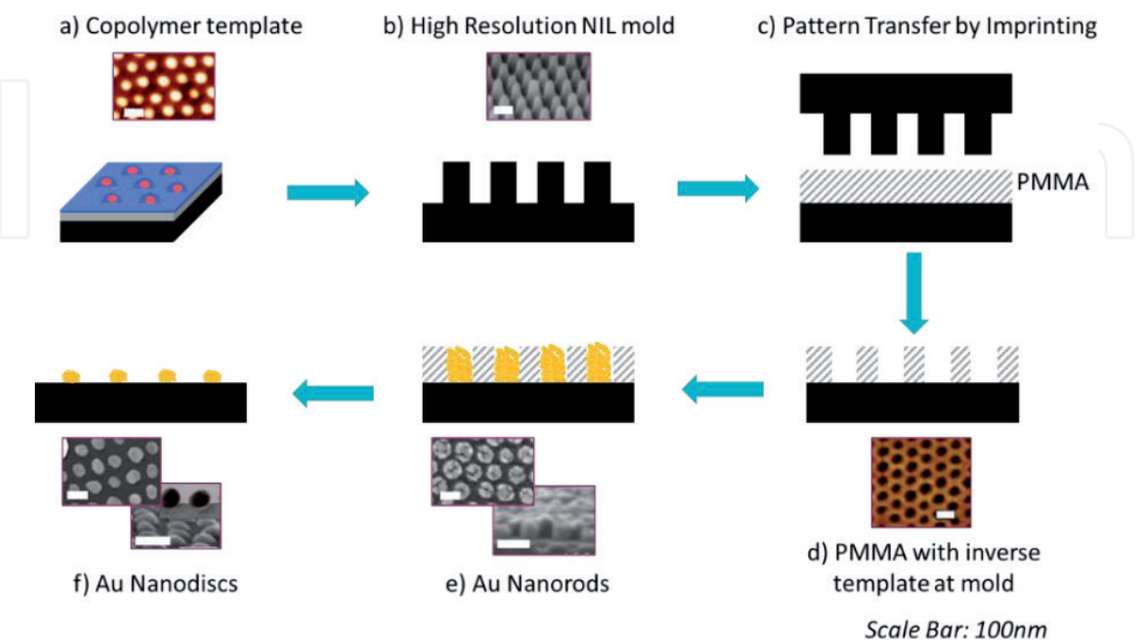

Figure 9.
Process steps involved in production of (a, b) high-resolution molds for NIL produced from self-assembled polymeric templates, (c, d) followed by replication onto PMMA thin film to form nanopore arrays and (e, f) selected area growth of gold nanorods within the pores and their subsequent transformation into nanodiscs [44].

while the nanodiscs remained undisturbed. Since our study primarily intended application of these arrays within a SERS-based sensor in liquid media, the nanorod arrays could not be considered further. Despite this instability, the nanorods could still find a use for plasmonic sensors functioning in the gas phase, or alternatively, if their mechanical stability can be improved through deposition of an overcoating of a dielectric, for example, alumina as shown earlier in literature [95]. The nanodisc arrays were evaluated for SERS performance against three different molecules, namely, naphthalene thiol that represented a covalently bound analyte, 2,2′-bipyridyl that represented non-covalently bound analyte, and crystal violet which represented the possibility of resonance Raman effect. The SERS performance was benchmarked against commercially available Klarite substrates and was proved better for all three molecules. The approach demonstrated an inherently reproducible approach to the fabrication of plasmonic arrays, as several copies can be derived starting from the same nanopillars NIL stamp. The performance of these arrays nevertheless has scope for improvements by further EM enhancements by reducing feature separations. The inability to deliver low feature separations is a limitation of the approach, which can be overcome by post-processing of the porous templates obtained after NIL, for instance, via pore-widening approaches.

4. Conclusions and outlook

Molecular self-assembly using amphiphilic copolymers and colloids derived thereof can deliver nanoplasmonic interfaces with high spatial resolutions, with control over geometric variables in steps of only a few nanometers. The approach enables metal nanoarrays with spatial coherence between features, orthogonal control over the different geometric attributes, and standard deviations below 10%. These characteristics can be leveraged to better understand and predict the optical properties of these arrays, allowing rational routes to maximize plasmonic sensing performance. The self-assembly parameters at both the template production and pattern transfer stages could be rigorously controlled to ensure high uniformity, reproducibility, and scalability of the resulting plasmonic arrays on full wafers. The correlation of the geometry ⇔ optical ⇔ SERS performance was demonstrated with a combination of experiments and numerical simulations. Plasmonic nanoarrays presenting a large number of gap hot spots, with gap distances down to sub-10 nm length scale, are possible to obtain in case of nanoparticle cluster arrays and nanopillar arrays. The homogeneously distributed hot spots over large areas present an opportunity to not only detect but also quantify the concentration of analytes, with large dynamic range with promisingly low limits of detection. Among the key challenges for future developments is to identify configurations that naturally drive the co-localization of analytes with EM hot spots to achieve maximize plasmonic signal enhancements. Further, the efforts to enhance EM fields solve only a part of the sensing challenge. In addition to maximizing the EM enhancements, the surface needs to be tailored to maximize analyte interactions and their concentrations on the surface.

Yet another challenge is the application of plasmonic arrays for biosensing. The high spatial resolutions sought for maximizing EM enhancements at gap or curvature hot spots are not compatible with the spatial requirements to accommodate large biomolecules like proteins. Further, the sensitivity of the plasmonic sensor extends typically to only a few nanometers from the surface. This is a challenge considering that the size of biomolecular interactions can already be a few tens of nanometers, for example, for an immunosandwich assay. Further, the plasmonic sensor needs to be adapted to work in complex media, for which the surface

functionalization to avoid non-specific binding would also consume part of the sensitive space above the plasmonic interface. While the plasmonic sensors have held high promise for highly sensitive, fast responding, and portable configurations, they need significant transversal development cutting across topics beyond fabrication, physics, and photonics, to ensure reliable devices that address emerging analytical challenges.

Acknowledgements

Funding received from National Research Fund of Luxembourg (FNR) via the project PLASENS (C15/MS/10459961) and FNR-PRIDE (FNR PRIDE/15/10935404) is gratefully acknowledged.

Author details

Rishabh Rastogi[1], Matteo Beggiato[1], Pierre Michel Adam[2], Saulius Juodkazis[3] and Sivashankar Krishnamoorthy[1*]

1 Materials Research and Technology Department, Luxembourg Institute of Science and Technology, Belvaux, Luxembourg

2 Institute Charles Delaunay CNRS, Physics, Mechanics, Materials and Nanotechnology, Department (PM2N), Nanotechnologies, Light, Nanomaterials and Nanotechnology team (L2N), University of Technology of Troyes (UTT), Troyes Cedex, France

3 Faculty of Science, Engineering and Technology, Swinburne University of Technology, Hawthorn, VIC, Australia

*Address all correspondence to: sivashankar.krishnamoorthy@list.lu

References

[1] Soler M, Huertas CS, Lechuga LM. Label-free plasmonic biosensors for point-of-care diagnostics: A review. Expert Review of Molecular Diagnostics. 2019;**19**(1):71-81

[2] Wabuyele MB et al. Portable Raman integrated tunable sensor (RAMiTs) for environmental field monitoring. Advanced Environmental, Chemical, and Biological Sensing Technologies II. 2004;**5586**:60

[3] Spencer KM, Sylvia JM, Marren PJ, Bertone JF, Christesen SD. Surface-enhanced Raman spectroscopy for homeland defense. Chemical and Biological Point Sensors for Homeland Defense. 2004;**5269**:1

[4] Bauch M, Toma K, Toma M, Zhang Q, Dostalek J. Plasmon-enhanced fluorescence biosensors: A review. Plasmonics. 2014;**9**(4):781-799

[5] Hammond JL, Bhalla N, Rafiee SD, Estrela P. Localized surface plasmon resonance as a biosensing platform for developing countries. Biosensors. 2014;**4**(2):172-188

[6] Maier SA, Atwater HA. Plasmonics: Localization and guiding of electromagnetic energy in metal/dielectric structures. Journal of Applied Physics. 2005;**98**(1):1-10

[7] Zhu W et al. Quantum mechanical effects in plasmonic structures with subnanometre gaps. Nature Communications. 2016;**7**:1-14

[8] Fang Y, Seong NH, Dlott DD. Measurement of the distribution of site enhancements in surface-enhanced raman scattering. Science. 2008;**321**(5887):388-392

[9] Balčytis A et al. From fundamental toward applied SERS: Shared principles and divergent approaches. Advanced Optical Materials. 2018;**6**(16):1-29

[10] Liu L et al. A high-performance and low cost SERS substrate of plasmonic nanopillars on plastic film fabricated by nanoimprint lithography with AAO template. AIP Advances. 2017;**7**(6):1-12

[11] Ye X et al. Improved size-tunable synthesis of monodisperse gold nanorods through the use of aromatic additives. ACS Nano. 2012;**6**(3):2804-2817

[12] Demirel MC et al. Bio-organism sensing via surface enhanced Raman spectroscopy on controlled metal/polymer nanostructured substrates. Biointerphases. 2009;**4**(2):35-41

[13] Chan S, Kwon S, Koo TW, Lee LP, Berlin AA. Surface-enhanced Raman scattering of small molecules from silver-coated silicon nanopores. Advanced Materials. 2003;**15**(19):1595-1598

[14] Kudelski A. Raman studies of rhodamine 6G and crystal violet sub-monolayers on electrochemically roughened silver substrates: Do dye molecules adsorb preferentially on highly SERS-active sites? Chemical Physics Letters. 2005;**414**(4-6):271-275

[15] Zeman EJ, Schatz GC. An accurate electromagnetic study of surface enhancement factors for Ag, Au, Cu, Li, Na, AI, Ga, In, Zn, and Cd. The Journal of Physical Chemistry. 1987;**91**(3):634-643

[16] Hildebrandt P, Stockhurger M. Surface-enhanced resonance Raman spectroscopy of Rhodamine 6G adsorbed on colloidal silver. The Journal of Physical Chemistry. 1984;**88**(24):5935-5944

[17] Huebner U, Boucher R, Schneidewind H, Cialla D, Popp J.

Microfabricated SERS-arrays with sharp-edged metallic nanostructures. Microelectronic Engineering. 2008;**85**(8):1792-1794

[18] Grand J et al. Optimization of SERS-active substrates for near-field Raman spectroscopy. Synthetic Metals. 2003;**139**(3):621-624

[19] Walsh GF, Forestiere C, Dal Negro L. Plasmon-enhanced depolarization of reflected light from arrays of nanoparticle dimers. Optics Express. 2011;**19**(21):21081

[20] Huang W, Yu X, Liu Y, Qiao W, Chen L. A review of the scalable nano-manufacturing technology for flexible devices. Frontiers of Mechanical Engineering. 2017;**12**(1):99-109

[21] Lim IIS et al. Adsorption of cyanine dyes on gold nanoparticles and formation of J-aggregates in the nanoparticle assembly. The Journal of Physical Chemistry. B. 2006;**110**(13):6673-6682

[22] Gaddis AL. Geometrical Effects on Electromagnetic Enhancement to SERS from Metal Nanoparticle Dimer Arrays. [Masters Theses]. Knoxville, USA: University of Tennessee; 2009:1-78

[23] Vazquez-Mena O et al. High-resolution resistless nanopatterning on polymer and flexible substrates for plasmonic biosensing using stencil masks. ACS Nano. 2012;**6**(6):5474-5481

[24] Chou SY, Krauss PR, Renstrom PJ. Imprint lithography with 25-nanometer resolution. Science. 1996;**272**(5258):85-87

[25] McNay G, Eustace D, Smith WE, Faulds K, Graham D. Surface-enhanced Raman scattering (SERS) and surface-enhanced resonance Raman scattering (SERRS): A review of applications. Applied Spectroscopy. 2011;**65**(8):825-837

[26] Sánchez-Iglesias A et al. Chemical seeded growth of Ag nanoparticle arrays and their application as reproducible SERS substrates. Nano Today. 2010;**5**(1):21-27

[27] Rekha CR, Sameera S, Nayar VU, Gopchandran KG. Simultaneous detection of different probe molecules using silver nanowires as SERS substrates. Spectrochimica Acta, Part A: Molecular and Biomolecular Spectroscopy. 2019;**213**(2018):150-158

[28] Krishnamoorthy S. Nanostructured sensors for biomedical applications-a current perspective. Current Opinion in Biotechnology. 2015;**34**:118-124

[29] Park S et al. Macroscopic 10 terabit/in 2 arrays from block copolymers with lateral order supplemental information. Science. 2009;**323**(February):1030

[30] Cheng JY, Ross CA, Thomas EL, Smith HI, Vancso GJ. Fabrication of nanostructures with long-range order using block copolymer lithography. Applied Physics Letters. 2002;**81**(19):3657-3659

[31] Stoykovich MP et al. Directed self-assembly of block copolymers for nanolithography: Fabrication of isolated features and essential integrated circuit geometries. ACS Nano. 2007;**1**(3):168-175

[32] Yang JKW et al. Complex self-assembled patterns using sparse commensurate templates with locally varying motifs. Nature Nanotechnology. 2010;**5**(4):256-260

[33] Cetin AE et al. Handheld high-throughput plasmonic biosensor using computational on-chip imaging. Light: Science & Applications. 2014;**3**(1)

[34] Aksu S, Yanik AA, Adato R, Artar A, Huang M, Altug H. High-throughput nanofabrication of infrared plasmonic nanoantenna arrays for

vibrational nanospectroscopy. Nano Letters. 2010;**10**(7):2511-2518

[35] Krishnamoorthy S, Manipaddy KK, Yap FL. Wafer-level self-organized copolymer templates for nanolithography with sub-50 nm feature and spatial resolutions. Advanced Functional Materials. 2011;**21**(6):1102-1112

[36] Krishnamoorthy S, Pugin R, Brugger J, Heinzelmann H, Hinderling C. Tuning the dimensions and periodicities of nanostructures starting from the same polystyrene-block-poly(2-vinylpyridine) diblock copolymer. Advanced Functional Materials. 2006;**16**(11):1469-1475

[37] Mansky P, Haikin P, Thomas EL. Monolayer films of diblock copolymer microdomains for nanolithographic applications. Journal of Materials Science. 1995;**30**(8):1987-1992

[38] Lu J, Chamberlin D, Rider DA, Liu M, Manners I, Russell TP. Using a ferrocenylsilane-based block copolymer as a template to produce nanotextured Ag surfaces: Uniformly enhanced surface enhanced Raman scattering active substrates. Nanotechnology. 2006;**17**(23):5792-5797

[39] Spatz JP, Sheiko S, Möller M. Substrate-induced lateral micro-phase separation of a diblock copolymer. Advanced Materials. 1996;**8**(6):513-517

[40] Letchford K, Burt H. A review of the formation and classification of amphiphilic block copolymer nanoparticulate structures: Micelles, nanospheres, nanocapsules and polymersomes. European Journal of Pharmaceutics and Biopharmaceutics. 2007;**65**(3):259-269

[41] Pedrosa CR et al. Controlled nanoscale topographies for osteogenic differentiation of mesenchymal stem cells. ACS Applied Materials & Interfaces. 2019;**11**(9):8858-8866

[42] Yap FL, Thoniyot P, Krishnan S, Krishnamoorthy S. Nanoparticle cluster arrays for high-performance SERS through directed self-assembly on flat substrates and on optical fibers. ACS Nano. 2012;**6**(3):2056-2070

[43] Dinda S, Suresh V, Thoniyot P, Balčytis A, Juodkazis S, Krishnamoorthy S. Engineering 3D nanoplasmonic assemblies for high performance spectroscopic sensing. ACS Applied Materials & Interfaces. 2015;**7**(50):27661-27666

[44] Krishnamoorthy S, Krishnan S, Thoniyot P, Low HY. Inherently reproducible fabrication of plasmonic nanoparticle arrays for SERS by combining nanoimprint and copolymer lithography. ACS Applied Materials & Interfaces. 2011;**3**(4):1033-1040

[45] Nordlander P, Oubre C, Prodan E, Li K, Stockman MI. Plasmon hybridization in nanoparticle dimers. Nano Letters. 2004;**4**(5):899-903

[46] Brandl DW, Mirin NA, Nordlander P. Plasmon modes of nanosphere trimers and quadrumers. The Journal of Physical Chemistry. B. 2006;**110**(25):12302-12310

[47] Hentschel M, Saliba M, Vogelgesang R, Giessen H, Alivisatos AP, Liu N. Transition from isolated to collective modes in plasmonic oligomers. Nano Letters. 2010;**10**(7):2721-2726

[48] Quinten M, Kreibig U. Optical properties of aggregates of small metal particles. Surface Science. 1986;**172**(3):557-577

[49] Mirin NA, Bao K, Nordlander P. Fano resonances in plasmonic nanoparticle aggregates. The

Journal of Physical Chemistry. A. 2009;**113**(16):4028-4034

[50] Natan MJ. Concluding remarks: Surface enhanced Raman scattering. Faraday Discussions. 2006;**132**:321

[51] Ueno K, Juodkazis S, Mizeikis V, Sasaki K, Misawa H. Clusters of closely spaced gold nanoparticles as a source of two-photon photoluminescence at visible wavelengths. Advanced Materials. 2008;**20**(1):26-30

[52] Fan JA et al. Fano-like interference in self-assembled plasmonic quadrumer clusters. Nano Letters. 2010;**10**(11):4680-4685

[53] Jin R. Nanoparticle clusters light up in SERS. Angewandte Chemie, International Edition. 2010;**49**(16):2826-2829

[54] Le F et al. Metallic nanoparticle arrays: A common substrate for both surface-enhanced Raman scattering and surface-enhanced infrared absorption. ACS Nano. 2008;**2**(4):707-718

[55] Lee JS, Ulmann PA, Han MS, Mirkin CA. A DNA - gold nanoparticle-based colorimetric competition assay for the detection of cysteine. Nano Letters. 2008;**8**(2):529-533

[56] Talley CE et al. Surface-enhanced Raman scattering from individual Au nanoparticles and nanoparticle dimer substrates. Nano Letters. 2005;**5**(8):1569-1574

[57] Camden JP et al. Probing the structure of single-molecule surface-enhanced Raman scattering hot spots. Journal of the American Chemical Society. 2008;**130**(38):12616-12617

[58] Lassiter JB et al. Fano resonances in plasmonic nanoclusters: Geometrical and chemical tunability. Nano Letters. 2010;**10**(8):3184-3189

[59] Ap A et al. Organization of nanocrystal molecules using DNA. Nature. 1996;**382**(6592):609-611

[60] Qiu P, Jensen C, Charity N, Towner R, Mao C. Oil phase evaporation-induced self-assembly of hydrophobic nanoparticles into spherical clusters with controlled surface chemistry in an oil-in-water dispersion and comparison of behaviors of individual and clustered iron oxide nanoparticles. Journal of the American Chemical Society. 2010;**132**(50):17724-17732

[61] Correa-Duarte MA, Liz-Marzán LM. Carbon nanotubes as templates for one-dimensional nanoparticle assemblies. Journal of Materials Chemistry. 2006;**16**(1):22-25

[62] Wang H, Lin W, Fritz KP, Scholes GD, Winnik MA, Manners I. Cylindrical block co-micelles with spatially selective functionalization by nanoparticles. Journal of the American Chemical Society. 2007;**129**(43):12924-12925

[63] Blum AS et al. Cowpea mosaic virus as a scaffold for 3-D patterning of gold nanoparticles. Nano Letters. 2004;**4**(5):867-870

[64] Lee W, Lee SY, Briber RM, Rabin O. Self-assembled SERS substrates with tunable surface plasmon resonances. Advanced Functional Materials. 2011;**21**(18):3424-3429

[65] Banwell CN, Sheppard N, Turner JJ. Directed deposition of nanoparticles using diblock copolymer templates. Advances in Molecular Spectroscopy. 2013;**15**(3):1183-1184

[66] Wang L, Montagne F, Hoffmann P, Heinzelmann H, Pugin R. Hierarchical positioning of gold nanoparticles into periodic arrays using block copolymer nanoring templates. Journal

of Colloid and Interface Science. 2011;**356**(2):496-504

[67] Förster S, Antonietti M. Amphiphilic block copolymers in structure-controlled nanomaterial hybrids. Advanced Materials. 1998;**10**(3):195-217

[68] Kugel V, Ji H-F. Nanopillars for sensing. Journal of Nanoscience and Nanotechnology. 2014;**14**(9):6469-6477

[69] Oh YJ, Kang M, Park M, Jeong KH. Engineering hot spots on plasmonic nanopillar arrays for SERS: A review. BioChip Journal. 2016;**10**(4):297-309

[70] Karadan P, Aggarwal S, Anappara AA,Narayana C, Barshilia HC. Tailored periodic Si nanopillar based architectures as highly sensitive universal SERS biosensing platform. Sensors Actuators, B Chemical. 2018;**254**:264-271

[71] Gudur A, Ji H-F. Bio-applications of nanopillars. Frontiers in Nanoscience and Nanotechnology. 2017;**2**(6):1-10

[72] Chattopadhyay S, Huang YF, Jen YJ, Ganguly A, Chen KH, Chen LC. Anti-reflecting and photonic nanostructures. Materials Science & Engineering R: Reports. 2010;**69**(1-3):1-35

[73] Zavaliche F et al. Electrically assisted magnetic recording in multiferroic nanostructures. Nano Letters. 2007;**7**(6):1586-1590

[74] Schneider L, Feidenhans'L NA, Telecka A, Taboryski RJ. One-step maskless fabrication and optical characterization of silicon surfaces with antireflective properties and a white color appearance. Scientific Reports. 2016;**6**(September):1-6

[75] Fujikawa S, Takaki R, Kunitake T. Fabrication of arrays of sub-20-nm silica walls via photolithography and solution-based molecular coating. Langmuir. 2006;**22**(21):9057-9061

[76] Cheung CL, Nikolić RJ, Reinhardt CE, Wang TF. Fabrication of nanopillars by nanosphere lithography. Nanotechnology. 2006;**17**(5):1339-1343

[77] Wang Y, Lee K, Irudayaraj J. Silver nanosphere SERS probes for sensitive identification of pathogens. Journal of Physical Chemistry C. 2010;**114**(39):16122-16128

[78] Dieringer JA et al. Surface enhanced Raman spectroscopy: New materials, concepts, characterization tools, and applications. Faraday Discussions. 2006;**132**:9-26

[79] Shiohara A, Wang Y, Liz-Marzán LM. Recent approaches toward creation of hot spots for SERS detection. Journal of Photochemistry and Photobiology C Photochemistry Reviews. 2014;**21**:2-25

[80] Kim JH, Kang T, Yoo SM, Lee SY, Kim B, Choi YK. A well-ordered flower-like gold nanostructure for integrated sensors via surface-enhanced Raman scattering. Nanotechnology. 2009;**20**(23):235302

[81] Duan H, Yang JKW, Berggren KK. Controlled collapse of high-aspect-ratio nanostructures. Small. 2011;**7**(18):2661-2668

[82] Lee SJ, Morrill AR, Moskovits M. Hot spots in silver nanowire bundles for surface-enhanced Raman spectroscopy. Journal of the American Chemical Society. 2006;**128**(7):2200-2201

[83] Chandra D, Yang S. Capillary-force-induced clustering of micropillar arrays: Is it caused by isolated capillary bridges or by the lateral capillary meniscus interaction force? Langmuir. 2009;**25**(18):10430-10434

[84] Gates BD, Xu Q, Thalladi VR, Cao T, Knickerbocker T, Whitesides GM. Shear patterning of microdominos: A new class of procedures for

making micro- and nanostructures. Angewandte Chemie, International Edition. 2004;**43**(21):2780-2783

[85] Hu M et al. Gold nanofingers for molecule trapping and detection. Journal of the American Chemical Society. 2010;**132**(37):12820-12822

[86] Schmidt MS, Hübner J, Boisen A. Large area fabrication of leaning silicon nanopillars for surface enhanced Raman spectroscopy. Advanced Materials. 2012;**24**(10):11-18

[87] Singh A, Knaepen W, Sayan S, El Otell Z, Chan BT, Maes JW, et al. Impact of sequential infiltration synthesis on pattern fidelity of DSA lines. In: Advances in Patterning Materials and Processes XXXII, Vol. 9425. International Society for Optics and Photonics; 2015. p. 94250N

[88] Ishchenko OM et al. Investigating sequential vapor infiltration synthesis on block-copolymer-templated titania nanoarrays. Journal of Physical Chemistry C. 2016;**120**(13):7067-7076

[89] Yin J, Xu Q, Wang Z, Yao X, Wang Y. Highly ordered TiO_2 nanostructures by sequential vapour infiltration of block copolymer micellar films in an atomic layer deposition reactor. Journal of Materials Chemistry C. 2013;**1**(5):1029-1036

[90] Ku SJ et al. Highly ordered freestanding titanium oxide nanotube arrays using Si-containing block copolymer lithography and atomic layer deposition. Nanotechnology. 2013;**24**(8):085301

[91] Peng Q, Tseng YC, Darling SB, Elam JW. Nanoscopic patterned materials with tunable dimensions via atomic layer deposition on block copolymers. Advanced Materials. 2010;**22**(45):5129-5133

[92] Guo LJ. Nanoimprint lithography: Methods and material requirements. Advanced Materials. 2007;**19**(4):495-513

[93] Aizawa M, Buriak JM. Block copolymer templated chemistry for the formation of metallic nanoparticle arrays on semiconductor surfaces. Chemistry of Materials. 2007;**19**(21):5090-5101

[94] Aizawa M, Buriak JM. Block copolymer-templated chemistry on Si, Ge, InP, and GaAs surfaces. Journal of the American Chemical Society. 2005;**127**(25):8932-8933

[95] Zhang X, Zhao J, Whitney AV, Elam JW, Van Duyne RP. Ultrastable substrates for surface-enhanced Raman spectroscopy: Al_2O_3 overlayers fabricated by atomic layer deposition yield improved anthrax biomarker detection. Journal of the American Chemical Society. 2006;**128**(31):10304-10309